ECCM 2010
IV European Conference on Computational Mechanics
Palais des Congrès, Paris, France, May 16-21, 2010

A continuous-discontinuous model for softening and cracking based on non-local displacements

Elena Tamayo-Mas and Antonio Rodríguez-Ferran

Laboratori de Càlcul Numèric (LaCàN)
Departament de Matemàtica Aplicada III
Escola Tècnica Superior d'Enginyers de Camins, Canals i Ports de Barcelona
Universitat Politècnica de Catalunya (UPC), Barcelona, Spain
{elena.tamayo,antonio.rodriguez-ferran}@upc.edu

Key words: Continuous-discontinuous strategy, non-local displacements, regularisation, softening, cracking, X-FEM

Summary. A continuous-discontinuous model to simulate numerically an entire failure process is presented. Crack inception and its propagation is modelled by means of a gradient non-local model based on non-local displacements. To simulate properly the final stages of the process, a discrete crack approach (X-FEM) is used, where both local and non-local displacements are modelled as discontinuous fields. In this paper, this new combined approach is studied in detail and one- and two-dimensional examples are carried out to validate it.

1 Introduction

In order to simulate numerically a failure process, either a continuous or a discontinuous approach may be used [1]. In continuum approaches, fracture is the result of a process of localisation and there is not any real discontinuity, while if a discontinuous approach is employed, displacement discontinuities are introduced into the model.

Continuous strategies are used to model the first stages of failure. If a local continuum model is employed, the numerical simulations present a pathological mesh sensitivity and physically unrealistic results are obtained [2]. To solve this mesh dependence, a regularisation technique must be used to incorporate non-locality into the model. A gradient-type model is used here, in which non-locality is introduced into the model via non-local displacements [3].

Nevertheless, if a non-local continuous model is used in the final stage of failure, numerical interaction between the separated parts of the body persists and unrealistic results may be obtained. Therefore, cracks must be introduced into the model. Here, the eXtended Finite Element Method (X-FEM) [4, 5] is used to model the growing cracks. By means of this method, the discontinuity is located independently of the finite element mesh [6] and remeshing as the crack grows is avoided [7].

In summary, in order to characterise numerically a whole failure process, a continuous-discontinuous approach is used, where a criterion determines the transition from the non-local continuum to a continuum with a discrete growing cohesive crack. Some strategies have been already proposed in the literature, see for example [8, 9, 10, 11].

In this work, the following strategy is presented. A non-local continuum damage model is used for the

continuum. When the damage parameter exceeds a threshold set a priori D_{crit}, a crack described by a cohesive law relating traction to displacement jump is introduced. The crack path is determined by the continuum: the steepest descent direction of the damage profile $-\nabla D$ is employed. Once the crack is introduced, the growing crack is modelled by means of X-FEM. In this model, the transition from a continuum to a discontinuous model is defined through an energy balance: damage value is fixed to D_{crit} and the bulk material unloads.

An outline of this paper follows. A continuous-discontinuous approach in standard media is reviewed in Section 2. The new model is presented in Section 3. The problem fields for a body crossed by a crack are described in Section 3.1. The governing equations and the variational formulation with its discretisation are derived in Sections 3.2 and 3.3 respectively. The regularisation capabilities of this new discontinuous strategy are illustrated in Section 4. First, the proposed approach is tested on a uniaxial tension test and then it is applied on a two-dimensional plate. The concluding remarks close this paper.

2 Continuous-discontinuous approach in standard media

This section deals with the continuous-discontinuous approach to failure. In this strategy, a continuous technique is used to simulate the first stages of failure up to the detection of a critical situation. When a critical situation is detected, a discontinuity is introduced and a continuous-discontinuous strategy is employed. The definition of critical situations depends on the underlying continuous model. In a damage continuum model, for example, a critical situation is reached when the damage parameter exceeds a critical damage value set a priori.

2.1 Problem fields

In X-FEM, the displacement field is approximated by the sum of a continuous and a discontinuous displacement field. The continuous part corresponds to the displacement field without any crack, while is the discontinuous or the enriched displacement field the additional displacement that models the discontinuities.

Consider a continuum body $\bar{\Omega}$ crossed by a discontinuity Γ_d, see Figure 1.

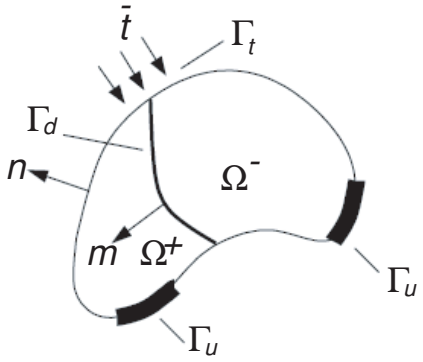

Figure 1: Body $\bar{\Omega}$ crossed by a discontinuity.

Then, the displacement field $\boldsymbol{u}$ can be decomposed as

$$\boldsymbol{u}(\boldsymbol{x}) = \boldsymbol{u}^1(\boldsymbol{x}) + \mathscr{H}_{\Gamma_d}(\boldsymbol{x})\boldsymbol{u}^2(\boldsymbol{x}) \tag{1}$$

where $\boldsymbol{u}^i(\boldsymbol{x})$ $(i = 1,2)$ are continuous fields and $\mathscr{H}_{\Gamma_d}$ is the Heaviside function centred at the discontinuity Γ_d. In the literature, different enrichment functions have been used, such as the Heaviside ([9, 10, 12])

or the sign function ([6, 7, 13, 14, 15]). In this work, the sign function

$$\mathscr{H}_{\Gamma_d}(\boldsymbol{x}) = \begin{cases} 1 & \text{if} \quad \boldsymbol{x} \in \bar{\Omega}^+ \\ -1 & \text{if} \quad \boldsymbol{x} \in \bar{\Omega}^- \end{cases} \tag{2}$$

(also called modified or generalised Heaviside function) centred at the discontinuity surface Γ_d is employed, because of its symmetry [7].

2.2 Governing equations

The equilibrium equations and boundary conditions for the body $\bar{\Omega}$ without body forces can be summarised as

$$\begin{aligned} \nabla \cdot \boldsymbol{\sigma} &= \mathbf{0} && \text{(3a)} \\ \boldsymbol{\sigma} \cdot \boldsymbol{n} &= \bar{\boldsymbol{t}} \quad \text{on} \Gamma_t && \text{(3b)} \\ \boldsymbol{\sigma} \cdot \boldsymbol{m} &= \boldsymbol{t} \quad \text{on} \Gamma_d && \text{(3c)} \\ \boldsymbol{u} &= \boldsymbol{u}^* \quad \text{on} \, \Gamma_{\boldsymbol{u}} && \text{(3d)} \end{aligned}$$

where $\boldsymbol{\sigma}$ is the Cauchy stress tensor, $\boldsymbol{n}$ is the outward unit normal to the body, $\boldsymbol{m}$ is the inward unit normal to Ω^+ on Γ_d, $\boldsymbol{u}^*$ is a prescribed displacement, $\bar{\boldsymbol{t}}$ is the load on the boundary, $\boldsymbol{t}$ is the load on the discontinuity surface and Γ_t and $\Gamma_{\boldsymbol{u}}$ are the surfaces with Neumann and Dirichlet boundary conditions respectively.

In order to solve this problem, a constitutive equation is needed to characterise the material. The constitutive equations for an elastic and a damage model are respectively

$$\begin{aligned} \boldsymbol{\sigma}(\boldsymbol{x},t) &= \mathbf{C} : \boldsymbol{\varepsilon}(\boldsymbol{x},t) && \text{(4a)} \\ \boldsymbol{\sigma}(\boldsymbol{x},t) &= [1 - D(\boldsymbol{x},t)]\, \mathbf{C} : \boldsymbol{\varepsilon}(\boldsymbol{x},t) && \text{(4b)} \end{aligned}$$

where $\boldsymbol{\varepsilon}$ is the small strain tensor, $\mathbf{C}$ the tensor of elastic moduli and D the damage parameter.

2.3 Variational formulation and finite element discretisation

In this section, the governing equations (3) are cast in a weak form. The space of trial local displacements is defined by the function

$$\boldsymbol{u}(\boldsymbol{x},t) = \boldsymbol{u}^1(\boldsymbol{x},t) + \mathscr{H}_{\Gamma_d}(\boldsymbol{x})\boldsymbol{u}^2(\mathbf{x},t), \qquad \boldsymbol{u}^1, \boldsymbol{u}^2 \in \mathscr{U}_{\boldsymbol{u}}, \tag{5}$$

where

$$\mathscr{U}_{\boldsymbol{u}} = \left\{ \boldsymbol{u}^1, \boldsymbol{u}^2 \mid \boldsymbol{u}^1, \boldsymbol{u}^2 \in H^1(\Omega) \text{ and } \boldsymbol{u}_{|\Gamma_{\boldsymbol{u}}} = \boldsymbol{u}^* \right\} \tag{6}$$

with $H^1(\Omega)$ a Sobolev space.

The equilibrium equation (3a) is multiplied by the weight function

$$\boldsymbol{\omega}(\boldsymbol{x},t) = \boldsymbol{\omega}^1(\boldsymbol{x},t) + \mathscr{H}_{\Gamma_d}(\boldsymbol{x})\boldsymbol{\omega}^2(\boldsymbol{x},t), \qquad \boldsymbol{\omega}^1, \boldsymbol{\omega}^2 \in \mathscr{W}_{\boldsymbol{u},\mathbf{0}} \tag{7}$$

with

$$\mathscr{W}_{\boldsymbol{u},\mathbf{0}} = \left\{ \boldsymbol{\omega}^1, \boldsymbol{\omega}^2 \mid \boldsymbol{\omega}^1, \boldsymbol{\omega}^2 \in H^1(\Omega) \text{ and } \boldsymbol{\omega}^1_{|\Gamma_u} = \boldsymbol{\omega}^2_{|\Gamma_u} = \mathbf{0} \right\}, \tag{8}$$

and integrated over the domain Ω to obtain the weak equilibrium statement. After standard manipulations, the following expressions are obtained:

$$\begin{aligned} &\int_\Omega \nabla^s \boldsymbol{\omega}^1 : \boldsymbol{\sigma} \, \mathrm{d}\Omega = \int_{\Gamma_t} \boldsymbol{\omega}^1 \cdot \bar{\boldsymbol{t}} \, \mathrm{d}\Gamma \qquad \forall \boldsymbol{\omega}^1 \in H^1(\Omega) && \text{(9a)} \\ &\int_\Omega \mathscr{H}_{\Gamma_d} \nabla^s \boldsymbol{\omega}^2 : \boldsymbol{\sigma} \, \mathrm{d}\Omega + 2\int_{\Gamma_d} \boldsymbol{\omega}^2 \cdot \boldsymbol{t} \, \mathrm{d}\Gamma = \int_{\Gamma_t} \mathscr{H}_{\Gamma_d} \boldsymbol{\omega}^2 \cdot \bar{\boldsymbol{t}} \, \mathrm{d}\Gamma \qquad \forall \boldsymbol{\omega}^2 \in H^1(\Omega) && \text{(9b)} \end{aligned}$$

where ∇^s is the symmetrised gradient and at the discontinuity,

$$\dot{\boldsymbol{t}} = \boldsymbol{T}[|\dot{\boldsymbol{u}}|] \tag{10}$$

where $\boldsymbol{T}$ relates traction rate $\dot{\boldsymbol{t}}$ and displacement jump rate $[|\dot{\boldsymbol{u}}|]$.

In FE analysis, using a Galerkin discretisation, Eq. (1) reads, for nodes whose support is crossed by Γ_d,

$$\mathbf{u}(\boldsymbol{x}) = \mathbf{N}(\boldsymbol{x})\mathbf{u}^1 + \mathscr{H}_{\Gamma_d}(\boldsymbol{x})\mathbf{N}(\boldsymbol{x})\mathbf{u}^2 \tag{11}$$

where $\mathbf{N}$ is the matrix of standard finite element shape functions, $\mathbf{u}^1$ are the basic nodal degrees of freedom and $\mathbf{u}^2$ are the enhanced ones.

The discrete format of the problem fields leads to the two discrete weak governing equations

$$\mathbf{f}_{\text{int},\mathbf{u}^1} = \mathbf{f}_{\text{ext},\mathbf{u}^1} \tag{12a}$$
$$\mathbf{f}_{\text{int},\mathbf{u}^2} = \mathbf{f}_{\text{ext},\mathbf{u}^2} \tag{12b}$$

where

$$\mathbf{f}_{\text{int},\mathbf{u}^1} = \int_\Omega \mathbf{B}^T\boldsymbol{\sigma}\,\mathrm{d}\Omega \tag{13a}$$
$$\mathbf{f}_{\text{ext},\mathbf{u}^1} = \int_{\Gamma_t} \mathbf{N}^T\bar{\boldsymbol{t}}\,\mathrm{d}\Gamma \tag{13b}$$
$$\mathbf{f}_{\text{int},\mathbf{u}^2} = \int_\Omega \mathscr{H}_{\Gamma_d}\mathbf{B}^T\boldsymbol{\sigma}\,\mathrm{d}\Omega + 2\int_{\Gamma_d} \mathbf{N}^T\boldsymbol{t}\,\mathrm{d}\Gamma \tag{13c}$$
$$\mathbf{f}_{\text{ext},\mathbf{u}^2} = \int_{\Gamma_t} \mathscr{H}_{\Gamma_d}\mathbf{N}^T\bar{\boldsymbol{t}}\,\mathrm{d}\Gamma \tag{13d}$$

with $\mathbf{B}$ the matrix of shape function derivatives. Some remarks about the discrete weak governing equations are worth mentioning:

- Eq. (12a) is the standard non-linear system of equilibrium equations, while Eq. (12b) takes into account the contribution of the crack.
- In Eq. (13c), the contribution of the crack is multiplied by a factor of two due to the chosen definition of the Heaviside function, see Eq. (2).

3 New continuous-discontinuous approach based on non-local displacements

The goal of this section is to present a new continuous-discontinuous strategy, which allows a realistic characterisation of the entire failure process. This strategy is based on a non-local model based on non-local displacements [3].

3.1 Problem fields

In the gradient-enhanced continuum model based on non-local displacements, two different displacements are used to formulate the model: the standard displacements $\boldsymbol{u}_a$ and the gradient-enriched displacements $\boldsymbol{u}_g$. By means of the X-FEM, both fields are represented as

$$\boldsymbol{u}_a(\boldsymbol{x}) = \boldsymbol{u}_a^1(\boldsymbol{x}) + \mathscr{H}_{\Gamma_d}(\boldsymbol{x})\boldsymbol{u}_a^2(\boldsymbol{x}) \tag{14a}$$
$$\boldsymbol{u}_g(\boldsymbol{x}) = \boldsymbol{u}_g^1(\boldsymbol{x}) + \mathscr{H}_{\Gamma_d}(\boldsymbol{x})\boldsymbol{u}_g^2(\boldsymbol{x}) \tag{14b}$$

where $\boldsymbol{u}_a^i(\boldsymbol{x})$ and $\boldsymbol{u}_g^i(\boldsymbol{x})$ $(i = 1,2)$ are continuous fields.

3.2 Governing equations

The equilibrium equations and boundary conditions for the body $\bar{\Omega}$ are summarised in Eq. (3). The constitutive equation for a damage continuum model is given by Eq. (4b). Moreover, in the non-local damage model based on non-local displacements, a second-order diffusion partial differential equation that relates non-local displacements $\boldsymbol{u}_g$ to local displacements $\boldsymbol{u}_a$ is added to the equilibrium equation

$$\boldsymbol{u}_g(\boldsymbol{x},t) - \ell^2 \nabla^2 \boldsymbol{u}_g(\boldsymbol{x},t) = \boldsymbol{u}_a(\boldsymbol{x},t) \qquad \text{in}\,\Omega \setminus \Gamma_d \tag{15}$$

where ℓ is the characteristic length of the non-local damage model.

To complete the coupled system of equations, boundary conditions at the boundary and at the discontinuity surface must be defined. Both for the continuous and the discontinuous displacement fields, combined boundary conditions are suggested here

$$\left.\begin{array}{rcl} \boldsymbol{u}_g^i \cdot \boldsymbol{n} & = & \boldsymbol{u}_a^i \cdot \boldsymbol{n} \\ \nabla\left(\boldsymbol{u}_g^i \cdot \boldsymbol{t}\right) \cdot \boldsymbol{n} & = & 0 \end{array}\right\} \text{on } \partial\Omega \qquad \left.\begin{array}{rcl} \boldsymbol{u}_g^i \cdot \boldsymbol{m} & = & \boldsymbol{u}_a^i \cdot \boldsymbol{m} \\ \nabla\left(\boldsymbol{u}_g^i \cdot \boldsymbol{t}\right) \cdot \boldsymbol{m} & = & 0 \end{array}\right\} \text{on } \Gamma_d \tag{16}$$

where $\boldsymbol{n}$ is the outward unit normal to the body and $\boldsymbol{m}$ is the inward unit normal to Ω^+ on Γ_d, see Figure 1.

3.3 Variational formulation and finite element discretisation

Similarly to Section 2.3, the space of trial non-local displacements $\boldsymbol{u}_g$ is defined by the function

$$\boldsymbol{u}_g(\boldsymbol{x},t) = \boldsymbol{u}_g^1(\boldsymbol{x},t) + \mathscr{H}_{\Gamma_d}(\boldsymbol{x})\boldsymbol{u}_g^2(\mathbf{x},t), \qquad \boldsymbol{u}_g^1, \boldsymbol{u}_g^2 \in \mathscr{U}_{\boldsymbol{u}}, \tag{17}$$

where $\mathscr{U}_{\mathbf{u}}$ is defined in Eq. (6).

Eq. (15) can be cast in a variational form by multiplication with a vector test function $\boldsymbol{\omega}(\boldsymbol{x},t)$ and integration over the domain Ω. After standard manipulations, one obtains

$$\begin{aligned} &\int_\Omega \boldsymbol{\omega}^1 \cdot \left(\boldsymbol{u}_g^1 + \mathscr{H}_{\Gamma_d}\boldsymbol{u}_g^2\right) \mathrm{d}\Omega + \ell^2 \int_\Omega \nabla\boldsymbol{\omega}^1 : \left(\nabla\boldsymbol{u}_g^1 + \mathscr{H}_{\Gamma_d}\nabla\boldsymbol{u}_g^2\right) \mathrm{d}\Omega - \ell^2 \int_{\Gamma_d} \mathscr{H}_{\Gamma_d}\boldsymbol{\omega}^1 \cdot \nabla\boldsymbol{u}_g^2 \boldsymbol{m}\,\mathrm{d}\Gamma \\ &-2\ell^2 \int_\Omega \boldsymbol{\omega}^1 \nabla\left(\delta_{\Gamma_d}\boldsymbol{m} \cdot \boldsymbol{u}_g^2\right) \mathrm{d}\Omega = \int_\Omega \boldsymbol{\omega}^1 \cdot \left(\boldsymbol{u}_a^1 + \mathscr{H}_{\Gamma_d}\boldsymbol{u}_a^2\right) \mathrm{d}\Omega \qquad \forall \boldsymbol{\omega}^1 \in \mathscr{W}_{\boldsymbol{u},\mathbf{0}} \end{aligned} \tag{18a}$$

$$\begin{aligned} &\int_\Omega \boldsymbol{\omega}^2 \cdot \left(\mathscr{H}_{\Gamma_d}\boldsymbol{u}_g^1 + \boldsymbol{u}_g^2\right) \mathrm{d}\Omega + \ell^2 \int_\Omega \nabla\boldsymbol{\omega}^2 : \left(\mathscr{H}_{\Gamma_d}\nabla\boldsymbol{u}_g^1 + \nabla\boldsymbol{u}_g^2\right) \mathrm{d}\Omega - \ell^2 \int_{\Gamma_d} \mathscr{H}_{\Gamma_d}\boldsymbol{\omega}^2 \cdot \nabla\boldsymbol{u}_g^1 \boldsymbol{m}\,\mathrm{d}\Gamma \\ &+2\ell^2 \int_\Omega \boldsymbol{\omega}^2 \cdot \left[\delta_{\Gamma_d}\boldsymbol{m}\left(\nabla\boldsymbol{u}_g^1 - \mathscr{H}_{\Gamma_d}\nabla\boldsymbol{u}_g^2\right) - \mathscr{H}_{\Gamma_d}\nabla\left(\delta_{\Gamma_d}\boldsymbol{m} \cdot \boldsymbol{u}_g^2\right)\right] \mathrm{d}\Omega = \int_\Omega \boldsymbol{\omega}^2 \cdot \left(\mathscr{H}_{\Gamma_d}\boldsymbol{u}_a^1 + \boldsymbol{u}_a^2\right) \mathrm{d}\Omega \\ &\qquad\qquad \forall \boldsymbol{\omega}^2 \in \mathscr{W}_{\boldsymbol{u},\mathbf{0}} \end{aligned} \tag{18b}$$

where δ_{Γ_d} is the Dirac delta centred at the discontinuity surface Γ_d.

Using FE notation, Eq. (14) reads, for nodes whose support is crossed by Γ_d,

$$\mathbf{u}_a(\boldsymbol{x}) = \mathbf{N}(\boldsymbol{x})\mathbf{u}_a^1(\boldsymbol{x}) + \mathscr{H}_{\Gamma_d}(\boldsymbol{x})\mathbf{N}(\boldsymbol{x})\mathbf{u}_a^2(\boldsymbol{x}) \tag{19a}$$

$$\mathbf{u}_g(\boldsymbol{x}) = \mathbf{N}(\boldsymbol{x})\mathbf{u}_g^1(\boldsymbol{x}) + \mathscr{H}_{\Gamma_d}(\boldsymbol{x})\mathbf{N}(\boldsymbol{x})\mathbf{u}_g^2(\boldsymbol{x}) \tag{19b}$$

and the discrete format of the problem fields leads to the two discrete weak governing equations

$$(\mathbf{M} + \ell^2\mathbf{D})\mathbf{u}_g^1 + (\mathbf{M}_{\mathscr{H}_{\Gamma_d}} + \ell^2\mathbf{D}_{\mathscr{H}_{\Gamma_d}})\mathbf{u}_g^2 = \mathbf{M}\mathbf{u}_a^1 + \mathbf{M}_{\mathscr{H}_{\Gamma_d}}\mathbf{u}_a^2 \tag{20a}$$

$$(\mathbf{M}_{\mathscr{H}_{\Gamma_d}} + \ell^2\mathbf{D}_{\mathscr{H}_{\Gamma_d}})\mathbf{u}_g^1 + (\mathbf{M} + \ell^2\mathbf{D})\mathbf{u}_g^2 = \mathbf{M}_{\mathscr{H}_{\Gamma_d}}\mathbf{u}_a^1 + \mathbf{M}\mathbf{u}_a^2 \tag{20b}$$

where

$$\begin{array}{rclcrcl} \mathbf{M} & = & \int_\Omega \mathbf{N}^T\mathbf{N}\,\mathrm{d}\Omega & & \mathbf{D} & = & \int_\Omega \nabla\mathbf{N}^T\nabla\mathbf{N}\,\mathrm{d}\Omega \\ \mathbf{M}_{\mathscr{H}_{\Gamma_d}} & = & \int_\Omega \mathscr{H}_{\Gamma_d}\mathbf{N}^T\mathbf{N}\,\mathrm{d}\Omega & & \mathbf{D}_{\mathscr{H}_{\Gamma_d}} & = & \int_\Omega \mathscr{H}_{\Gamma_d}\nabla\mathbf{N}^T\nabla\mathbf{N}\,\mathrm{d}\Omega \end{array} \tag{21}$$

Some remarks about the discretisation:

- Matrices $\mathbf{M}$ and $\mathbf{D}$ are the mass and diffusivity matrices already obtained in [3]. They are both constant.
- Matrices $\mathbf{M}_{\mathscr{H}_{\Gamma_d}}$ and $\mathbf{D}_{\mathscr{H}_{\Gamma_d}}$ can be understood as enriched mass and diffusivity matrices respectively, since the expression is the same as $\mathbf{M}$ and $\mathbf{D}$ except for the Heaviside function.
- Note that the property $\mathscr{H}_{\Gamma_d}\mathscr{H}_{\Gamma_d} = +1$, which is derived from the definition of the Heaviside function Eq. (2), is used.

4 Numerical results

The regularisation capabilities of this new strategy are illustrated in this section by means of two numerical examples. In section 4.1, a uniaxial tension test is carried out using a one- and two-dimensional geometry and in section 4.2, a two-dimensional square plate under mode I loading conditions is analysed.

4.1 Uniaxial tension test

This first example deals with the solution of a bar in tension with a discontinuity in the centre subjected to imposed displacement at the free side and clamped at the other one, see Figure 2. Since in the first steps of the failure process a continuum damage model is used, the central tenth of the bar is weakened to cause localisation. The dimensionless geometric and material parameters for this test are summarised in Table 1. All numerical tests have been carried out with one- and two-dimensional finite elements.

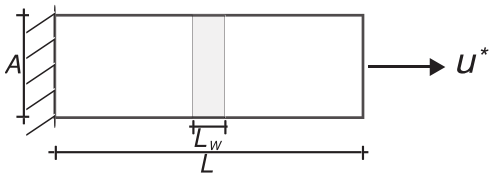

Figure 2: Uniaxial tension test: problem statement.

Table 1: Uniaxial tension test with a non-local damage model and a softening behaviour of the cohesive crack: geometric and material parameters.

Meaning	Symbol	Value
Length of the bar	L	100
Width of the bar	A	1
Length of weaker part	L_W	$L/7$
Young's modulus	E	20 000
Idem of weaker part	E_W	18 000
Damage threshold	ε_i	10^{-4}
Final strain	ε_f	1.25×10^{-2}
Critical damage	D_{crit}	0.9
Crack stiffness	T	-20

A non-local continuum damage model (linear softening law) is employed in the first stages of the failure process. When the damage parameter exceeds a threshold set a priori called D_{crit}, a discontinuity is introduced and the continuous-discontinuous technique is used, see Figure 3.

The regularisation properties of the model are analysed by means of different tests. As a first test, a fixed characteristic length $\ell = \sqrt{5}$ is chosen. The analysis is carried out with six different meshes. The

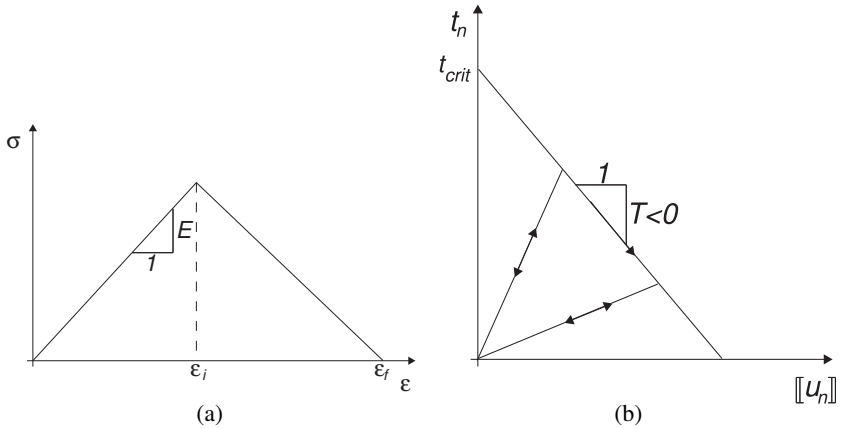

Figure 3: Evolution law for (a) the bar; (b) the crack.

force-displacement curves and the damage profiles are shown in Figure 4. As desired, the responses for this test do not depend on finite element sizes.

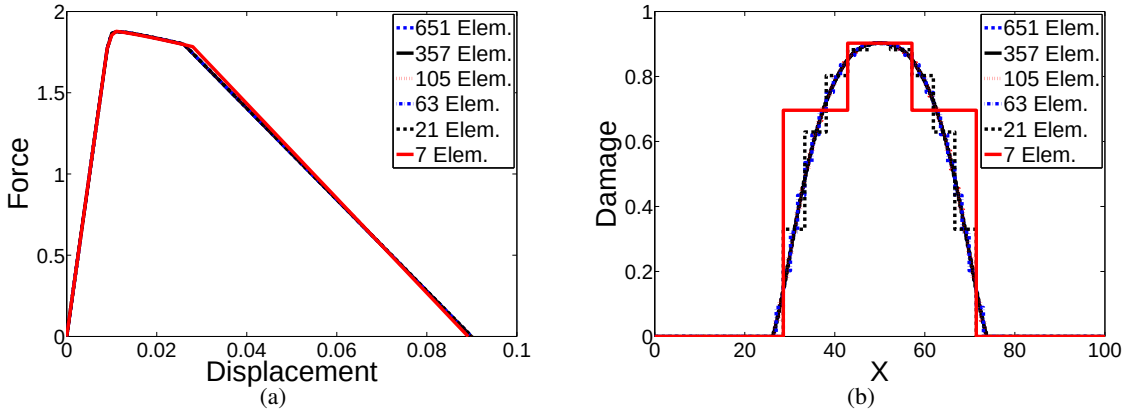

Figure 4: Continuous-discontinuous strategy. Fixed characteristic length with various meshes. (a) force-displacement curve; (b) damage profiles.

As a second test, a fixed mesh of 105 elements is considered and four different characteristic lengths are used, $\ell = \sqrt{1}, \sqrt{2}, \sqrt{5}, \sqrt{10}$. The results are depicted in Figure 5. The ductility in the force-displacement response and the width of the final damage profile increase with the internal length scale.

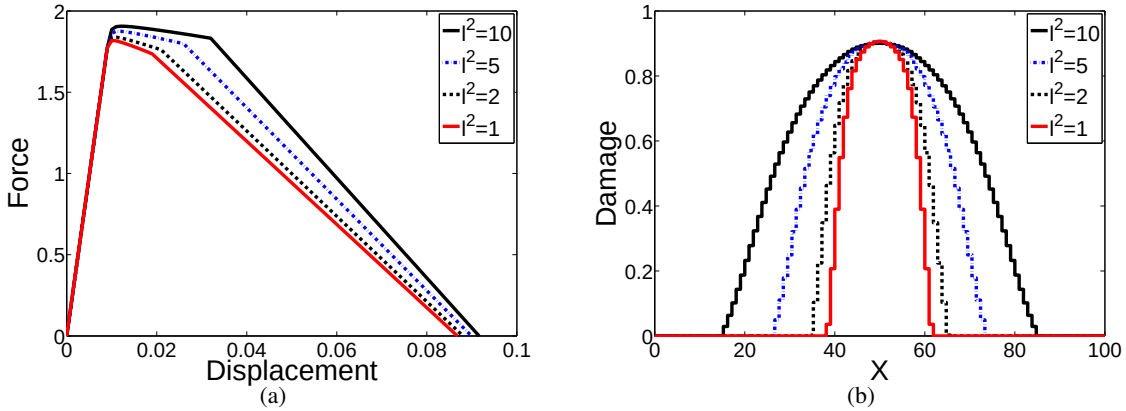

Figure 5: Continuous-discontinuous strategy. Fixed mesh with various characteristic lengths. (a) force-displacement curve; (b) damage profiles.

Finally, as a third test, a fixed mesh of 105 elements and a fixed characteristic length $\ell = \sqrt{5}$ are chosen.

Two different tests, in which the size of weakened region differs, are analysed. Results are shown in Figure 6. As seen, there is no pathological dependence on imperfection size.

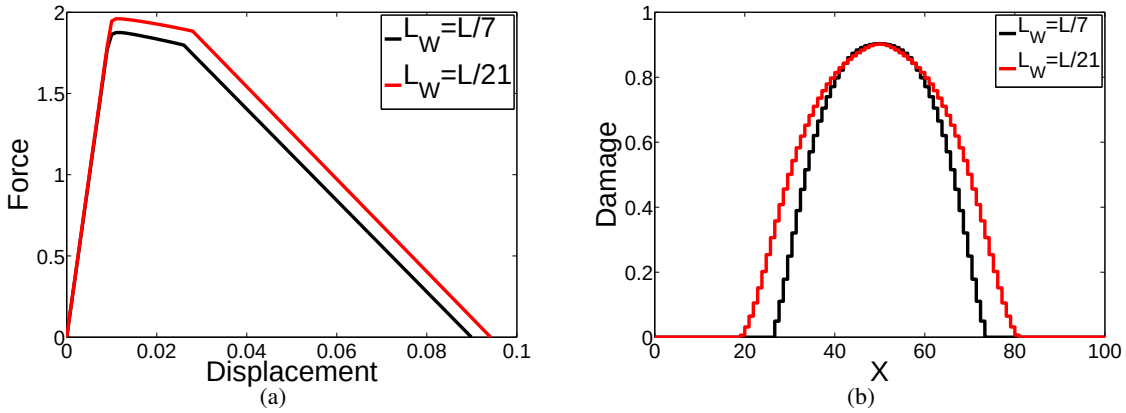

(a) (b)

Figure 6: Continuous-discontinuous strategy. Fixed mesh and characteristic length with various imperfection sizes. (a) force-displacement curve; (b) damage profiles.

In summary, this new model exhibits the desired regularisation capabilities.

4.2 Square plate under mode I loading conditions

The second example consists of a square plate under mode I loading conditions, see Figure 7. Similarly to the previous example, in order to simulate the first steps of the failure process with a continuum damage model, some weakened region is considered. The dimensionless geometric and material parameters for this test are summarised in Table 2.

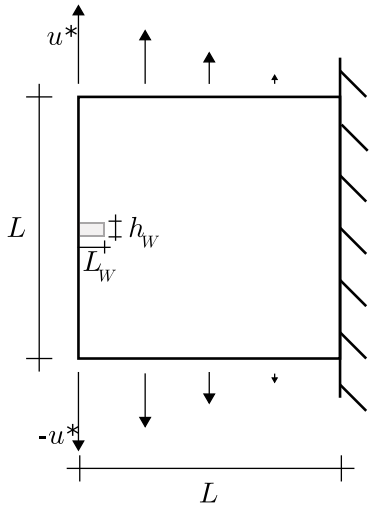

Figure 7: Square plate under mode I loading conditions: problem statement.

As a first test, the regularisation capabilities of the continuous strategy are analysed. Three different meshes are considered. The force-displacement curves and the damage profiles are shown in Figure 8 and 9 respectively. As seen, the force-displacement curve and the width of damage band do not depend on the finite element mesh or the imperfection size needed to cause localisation.

As a second test, the continuous-discontinuous strategy is analysed. A fixed mesh of 20×21 elements is considered. The force-displacement curve and the damage profile can be seen in Figure 10. As observed in Figure 10(a), the force-displacement curve presents sharp unloadings followed by loadings of the force. These unloadings, that occur when the crack propagates through the finite element mesh, are not

Table 2: Two-dimensional test under mode I loading conditions with a non-local damage model and a softening behaviour of the cohesive crack: geometric and material parameters.

Meaning	Symbol	Value
Length of the specimen	L	10
Length of weaker part	L_W	1
Width of weaker part	h_W	1 finite element
Young's modulus	E	20 000
Idem of weaker part	E_W	18 000 (10% reduction in E)
Poisson's coefficient	ν	0
Damage threshold	ε_i	10^{-4}
Final strain	ε_f	1.25×10^{-2}
Characteristic length	l	$\sqrt{7 \times 10^{-4}}$
Critical damage	D_{crit}	0.95
Crack stiffness	T	-20

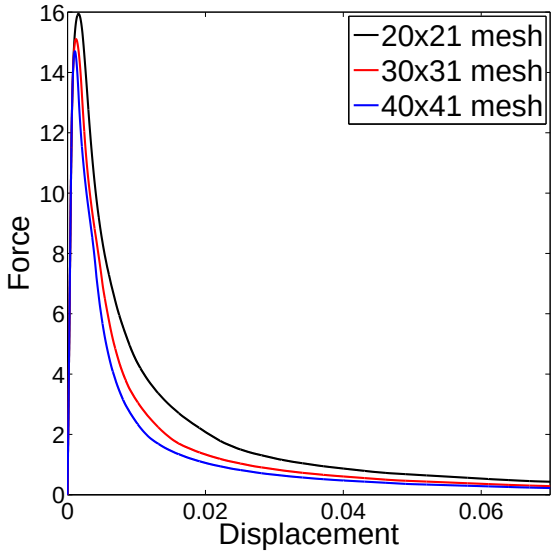

Figure 8: Continuous strategy. Fixed characteristic length with various meshes and imperfection sizes: force-displacement curves.

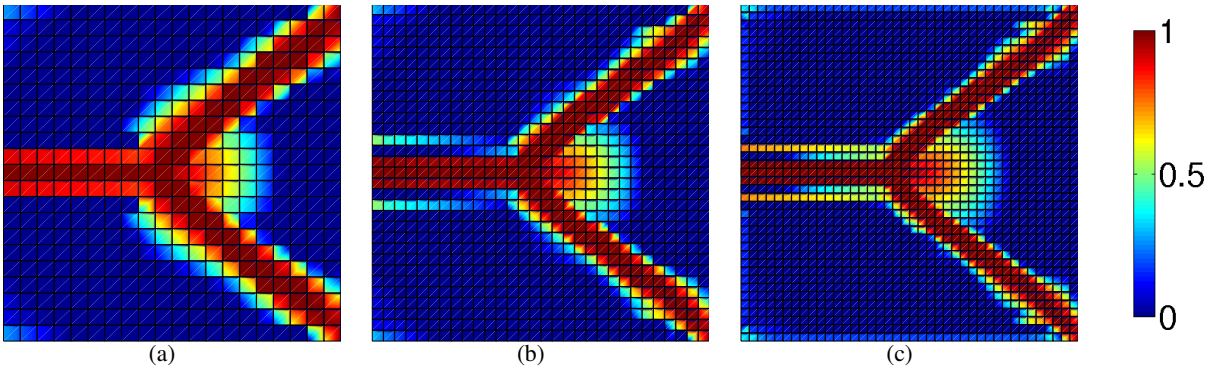

Figure 9: Continuous strategy. Fixed characteristic length with various meshes and imperfection sizes: damage profiles obtained with a (a) 20×21 FE mesh; (b) 30×31 FE mesh; (c) 40×41 FE mesh.

completely understood yet but we think that they may be related to the effect of the blending elements, as discussed next.

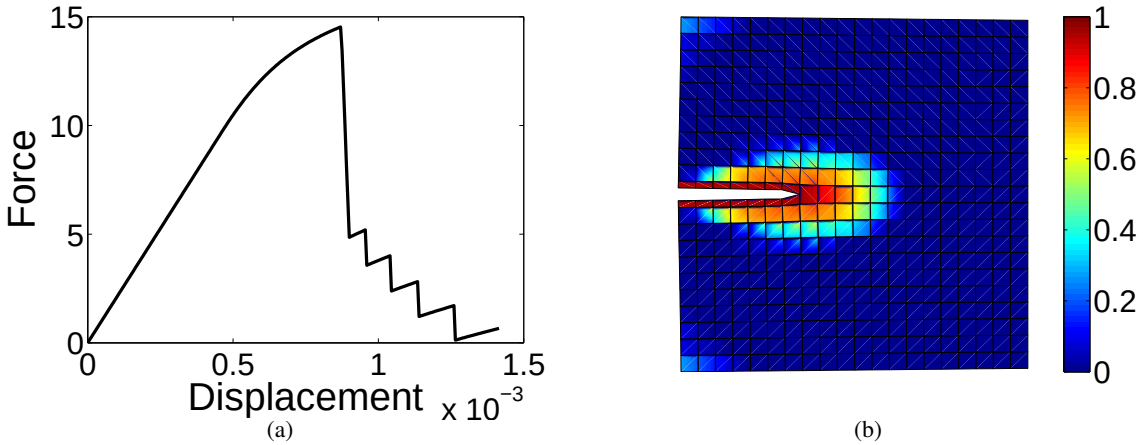

(a) (b)

Figure 10: Continuous-discontinuous strategy. (a) force-displacement curve; (b) damage profile with the deformed mesh (displacements amplified 100 times).

4.3 Blending elements

In X-FEM, the approximation function space of standard finite element methods (FEM) is expanded in order to deal with singularities. Although this enrichment could affect the entire domain, for computational purposes it is done only in the sub-domain where it is needed. Due to this local enrichment, three different kinds of elements exist: (a) standard elements with no enriched nodes, (b) elements whose nodes are all enriched and (c) elements with some of their nodes enriched, which are commonly named *blending elements*, see Figure 11. The influence of the blending elements on the solution accuracy has been reported in the literature, see for example [16, 17, 18].

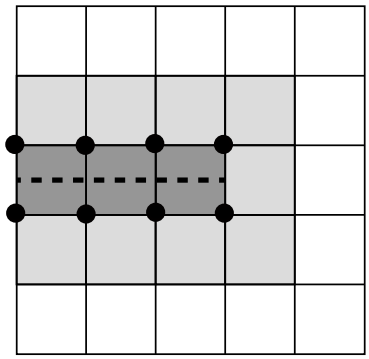

Figure 11: A crack line (dashed line) in a structured mesh with standard elements (white), elements whose nodes are all enriched (dark grey) and blending elements (light grey).

In this section, the stiffness of these types of elements is analysed via three different tests that deal with the solution of a two-dimensional plate in tension. The plate is discretised with one finite element and the numerical tests are displacement-controlled, see Figure 12.

The dimensionless geometric and material parameters used in this example are summarised in Table 3. Some remarks about the definition of these parameters are worth mentioning:

- $\varepsilon_{\text{crit}} = \varepsilon(D = D_{\text{crit}}) = \frac{\varepsilon_i \varepsilon_f}{\varepsilon_i + (1 - D_{\text{crit}})(\varepsilon_f - \varepsilon_i)}$, if a linear damage law is assumed, see Figure 3(a).
- The crack stiffness T has been defined imposing that the force-displacement curves in test 12(a) and 12(b) are equal. That means that all the imposed displacement is used for bulk deformation in the first case while in the second one, it is used for crack opening.

The obtained force-displacement curves are shown in Figure 13. Due to the definition of the crack stiff-

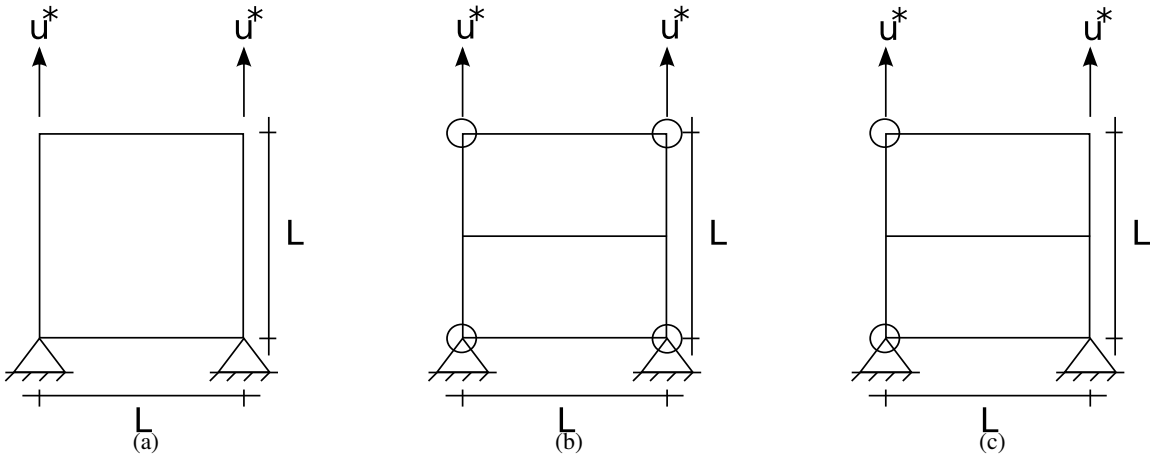

Figure 12: (a) element with standard nodes; (b) element with all the nodes enriched; (c) element with some of the nodes enriched.

Table 3: Effect of the blending elements in the global response: geometric and material parameters.

Meaning	Symbol	Value
Length of the specimen	L	1
Young's modulus	E	20000
Poisson's coefficient	ν	0
Damage threshold	ε_i	10^{-4}
Final strain	ε_f	1.25×10^{-2}
Characteristic length	l	0 (local model)
Critical damage	D_{crit}	0.9
Crack stiffness	T	$-\frac{(1-D_{\text{crit}})E\varepsilon_{\text{crit}}}{L\varepsilon_f}$

ness T, the force-displacement curves related to continuous and fully continuous-discontinuous elements are overlapped. Nevertheless, the curve related to the blending element has a different slope in the third branch, where the crack is introduced. It may be seen that the blending element offers a stiffer response in comparison with the other two elements. Depending on the geometric and material parameters, the behaviour of the blending element may be so stiff that the global response is not in softening but in hardening.

5 Concluding remarks

- The proposed continuous-discontinuous model is only based on displacements: a local displacement and a gradient-enriched field are used. In the final stage of the failure process, the two displacement fields may admit discontinuities. The two fields can be interpolated using the same shape and enrichment functions. Considering both fields discontinuous, relatively coarse meshes can be employed.

- When a crack is introduced, the discontinuous setting coexists with the continuous one. In fact, here the continuum is used for crack path tracking.

- On the one hand, a one-dimensional problem is analysed in order to validate the proposed strategy. The expected regularisation capabilities of the continuous-discontinuous model are obtained.

- On the other hand, a two-dimensional problem under mode I loading conditions is studied. By means of this example, it may be seen that the continuous model based on non-local displacements does regularise softening. Nevertheless, the force-displacement curve obtained with the

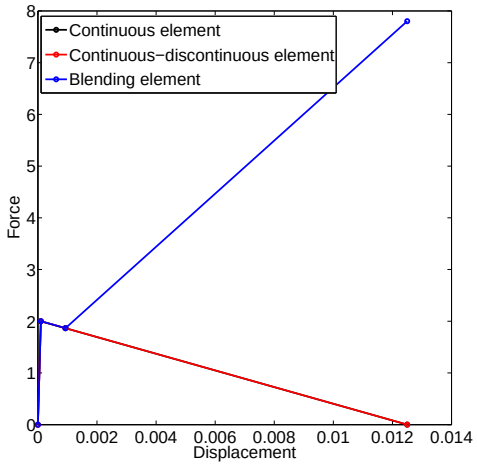

Figure 13: Effect of the blending elements in the global response: force-displacement curves.

continuous-discontinuous approach shows some sharp unloadings that require a better understanding. Since we think that this physically unrealistic behaviour is related to the blending elements, these are studied in detail.

References

[1] J. Oliver, A.E. Huespe, M.D.G Pulido, and E. Chaves. From continuum mechanics to fracture mechanics: the strong discontinuity approach. *Engineering Fracture Mechanics*, 69(2):113–136, 2002.

[2] M. Jirásek. Nonlocal damage mechanics. *Revue Européenne de Génie Civil*, 11(7-8):993–1021, 2007.

[3] A. Rodríguez-Ferran, I. Morata, and A. Huerta. A new damage model based on non-local displacements. *International Journal for Numerical and Analytical Methods in Geomechanics*, 29(5):473–493, 2005.

[4] T. Belytschko and T. Black. Elastic crack growth in finite elements with minimal remeshing. *International Journal for Numerical Methods in Engineering*, 45(5):601–620, 1999.

[5] N. Moes, J. Dolbow, and T. Belytschko. A finite element method for crack growth without remeshing. *International Journal for Numerical Methods in Engineering*, 46(1):131–150, 1999.

[6] N. Moes and T. Belytschko. Extended finite element method for cohesive crack growth. *Engineering Fracture Mechanics*, 69(7):813–833, 2002.

[7] G. Zi and T. Belytschko. New crack-tip elements for XFEM and applications to cohesive cracks. *International Journal for Numerical Methods in Engineering*, 57(15):2221–2240, 2003.

[8] C. Comi, S. Mariani, and U. Perego. An extended FE strategy for transition from continuum damage to mode I cohesive crack propagation. *International Journal for Numerical and Analytical Methods in Geomechanics*, 31(2):213–238, 2007.

[9] A. Simone, G.N. Wells, and L.J. Sluys. From continuous to discontinuous failure in a gradient-enhanced continuum damage model. *Computer Methods in Applied Mechanics and Engineering*, 192(41-42):4581–4607, 2003.

[10] G.N. Wells, L.J. Sluys, and R. De Borst. Simulating the propagation of displacement discontinuities in a regularized strain-softening medium. *International Journal for Numerical Methods in Engineering*, 53(5):1235–1256, 2002.

[11] E. Benvenuti. A regularized XFEM framework for embedded cohesive interfaces. *Computer Methods in Applied Mechanics and Engineering*, 197(49-50):4367–4378, 2008.

[12] G.N. Wells and L.J. Sluys. A new method for modelling cohesive cracks using finite elements. *International Journal for Numerical Methods in Engineering*, 50(12):2667–2682, 2001.

[13] C. Comi and S. Mariani. Extended finite element simulation of quasi-brittle fracture in functionally graded materials. *Computer Methods in Applied Mechanics and Engineering*, 196(41-44):4013–4026, 2007.

[14] E. Bechet, H. Minnebo, N. Moes, and B. Burgardt. Improved implementation and robustness study of the X-FEM for stress analysis around cracks. *International Journal for Numerical Methods in Engineering*, 64(8):1033–1056, 2005.

[15] S. Mariani and U. Perego. Extended finite element method for quasi-brittle fracture. *International Journal for Numerical Methods in Engineering*, 58(1):103–126, 2003.

[16] T.P. Fries. A corrected XFEM approximation without problems in blending elements. *International Journal for Numerical Methods in Engineering*, 75(5):503–532, 2008.

[17] J. Chessa, H. Wang, and T. Belytschko. On the construction of blending elements for local partition of unity enriched finite elements. *International Journal for Numerical Methods in Engineering*, 57(7):1015–1038, 2003.

[18] R. Gracie, H. Wang, and T. Belytschko. Blending in the extended finite element method by discontinuous galerkin and assumed strain methods. *International Journal for Numerical Methods in Engineering*, 74(11):1645–1669, 2008.

With the support of Universitat Politècnica de Catalunya (UPC).